J Mater Sci (2006) 41:5480–5489
DOI 10.1007/s10853-006-0338-7

Studies on sintering behaviour of Al_2O_3–ZrO_2 oxide composites processed by extended arc thermal plasma and conventional heating

D. R. Sahu · B. K. Roul · S. K. Singh · R. N. P. Choudhury

Received: 23 March 2005 / Accepted: 30 September 2005 / Published online: 17 June 2006

Abstract Al_2O_3–ZrO_2 composites were sintered using low cost extended arc thermal plasma reactor and conventional heating. Composites prepared in a wide range of composition were studied in terms of their density, shrinkage, hardness, structure, microstructure and dielectric response. Experimental parameter such as sintering time, sintering temperature and plasma power were optimized to achieve higher sintered end product. Highly dense sintered products were obtained by plasma heating route within short sintering time compared with conventional sintered method. Interesting development pertaining to structure and phase evolution, structure and dielectric response are analyzed. It is found that compositional variation in this composite produces structural phase separation at different sintering conditions, which is more in plasma heating product than conventional heated product. Plasma sintered product always shows less dielectric constant as compared to conventional sintered sample.

D. R. Sahu (✉)
Department of Materials Science and Engineering, National Cheng Kung University, Tainan 701, Taiwan
e-mail: sahu@mail.ncku.edu.tw

B. K. Roul · D. R. Sahu
Institute of Materials Science, Bhubaneswar 751013, India

S. K. Singh
Regional Research Laboratory, Bhubaneswar 751013, India

R. N. P. Choudhury
Department of Physics and Meteorology, Indian Institute of Technology, Kharagpur 721302, India

Introduction

Modern need for producing exotic new materials [1–3] having desired specific properties are primary challenges for scientist and engineers. With the advent of modern material processing technology, it is possible to prepare specific ceramics materials with desired dimension having density nearer to theoretical value including its original properties required for different mechanical, tribiological, structural and electronic applications. Based on different new ceramic processing techniques [4–6], using different processing route [7–10], many new advanced ceramic composite materials have been generated. However, Al_2O_3 and ZrO_2 are believed to be the base materials for different types of ceramics ranging from structural [11, 12] to biomaterials [13–15] use. Development and processing of different composites based on this material are very much essential for its applications. Although the same materials have been developed individually at different times [15–18], its composites have not yet been investigated thoroughly so far as its processing technology is concerned. Again vigorous and heavy competitions are seen to be dominated in the global marketplace in connection with critical issues like inexpensive process technology, time and energy saving during processing and reproducibility factor. Further to it, in many ceramic system processed by sintering of powder compacts, both full density and fine grained structure in sintered end product are essential. But, simultaneous attainment of these two objectives appears to be difficult, because grain-coarsening always follow the physical densification during sintering. Hence rapid sintering process [19–23] that requires very much shorter duration is likely to be an ideal approach. In order to resolve these issues, heating sources like laser, microwave and plasma are used which are considered to be exhibited

high heat and mass transfer kinetics during material processing. Among these three heating source, plasma heating source appear to be simple and inexpensive due to the recent development of low cost and easy plasma instrumentations. Keeping on these above view, this paper presents the sintering behaviour of Al_2O_3–ZrO_2 oxide composites using extended arc thermal plasma heating (EATPH) reactor and conventional heating. The primary objective of this paper is to investigate the possibility of processing the composites based on Al_2O_3 and ZrO_2 using unconventional novel route by plasma and to study its properties for the development of these materials in detail. It is observed that EATPH source can be more effective for sintering of Al_x–Zr_{100-x} (x = 0, 10, 20...) oxide composites than conventional heating.

Experimental

Commercial grade Al_2O_3 having chemical composition (α-alumina + TiO_2 < 0.01% + Fe_2O_3 < 0.003) and ZrO_2 (m-ZrO_2 + Na_2O < 0.01% + SiO_2 < 0.05%) with purity 99.99% were taken to prepare samples of different composition. The compositions of Al_x–Zr_{100-x} oxides was taken with different x (x = 0, 10, 20...100). The respective powders were mixed thoroughly and heated at 500 °C for 8 h. The powders were mixed with polyvinyl alcohol (PVA, 1 wt%) and pressed into pellets having 5 g weight and 10 mm diameter, at a pressure of about 8 T/cm^2. The pellets thus prepared were heated upto 800 °C, to remove the PVA binder and other low temperature volatiles (if present) and then used for sintering by resistive conventional heating and extended arc thermal plasma heating. One extended arc thermal plasma heating system has been designed and fabricated [24] using 30 kW DC power supply which is also presented in Fig. 1. Water-cooled stainless steel double wall cylindrical chamber (outer) is fixed with suitable thermal insulation by bubble alumina for the confinement of plasma heating. Provisions are made for fine adjustment of the electrode distance to get required arc length. Plasmagen gas (argon) flow into the electrode space is provided through a narrow hole through upper electrode (cathode). Sample holder is placed coaxially between the electrodes. High pressure cooled water is allowed to flow through out the external body of the reactor. Heavy weight graphite base is placed nearer to the sample holder to hold the temperature of this arching zone of the plasma reactor. Diameters of the sample holders are varied with respect to the diameter of the upper electrode for maintaining uniform and suitable arc zone. Rack and pinion arrangements are incorporated with the reactor vessel in order to control accurately the plasma arc length and plasma sustainability under particular plasma power. Details of the reactor was placed elsewhere [24–27]. Calcined samples of Al_2O_3–ZrO_2 in the pellet form were placed symmetrically inside the sample holder and fixed coaxially to the lower electrode w.r.t to the cathode. Graphite sample holders were used which were placed coaxially along the plasma arc length. Plasma power and argon gas flow through the electrode, plasma-sintering time were varied to study the sintering characteristics of the material. All pellets (presintered and sintered by conventional and thermal plasma) were taken for density measurement using Archimedes principle with deionized water as the immersion medium. XRD of the samples were carried out in the range of 2θ = 10–80° using CuK_α radiation by a Philip diffractometer (Model PW 1715) fitted with a monochromatometer and operated at 40 kV and 20 mA. The microstructure of the sintered bodies were studied by Scanning Electron Microscope (JEOL-35CF). The hardness was evaluated by the Vickers indentation method. Dielectric studies were performed by GR 1620 dielectric bridge with different frequencies and temperature.

Results and discussion

Calcination of the composites

In order to maintain uniformity in carrying out sintering studies, all samples were calcined at 800 °C for 10 h and used for both conventional as well as extend arc thermal plasma heating. Identical behaviour was observed in respect of all samples. Approximately 36–70% (approximately) of density was achieved by heating at 800 °C for 10 h for almost each pellet. At this density level, all samples become plasma and conventional heating compatible.

Density

Densification of the pellets having composition Al_x–Zr_{100-x} (x = 0, 10, 20...100) were carried out using conventional heating at different temperature for fixed 20 h of sintering time and at different plasma power with fixed sintering time of 15 min using plasma heating are presented in Fig. 2a, b respectively. It is observed that at x = 0 (only ZrO_2) shows highest density (96% of the theoretical value) within 15 min of sintering time using 25 kW of plasma power. However, the value of plasma sintered density is decreased as the value of x is increased and is noted to be minimum for pure Al_2O_3. Similar densification behaviour was also observed using conventional heating for 20 h. It is evident from Fig. 2a, b that identical compositions of the Al_2O_3–ZrO_2 composites were sintered to high density (~96% of theoretical value) in few minutes by plasma heating instead of high temperature (~1600 °C) conventional heating which

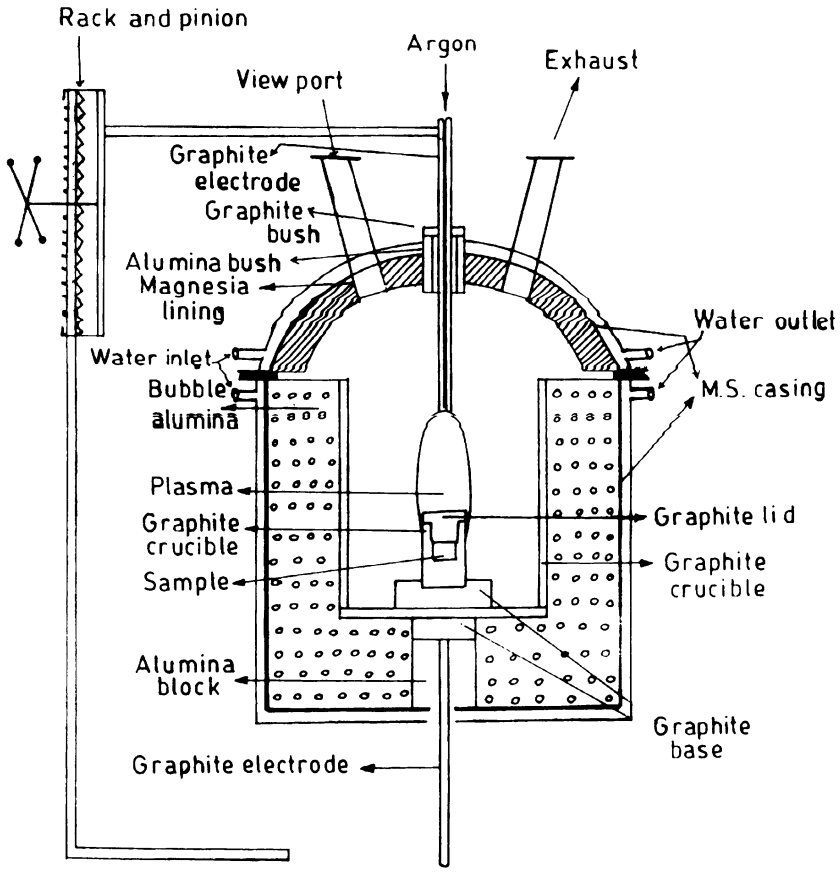

Fig. 1 Block diagram of an extended arc thermal plasma reactor

take a few tens of hours (20 h). This result shows that sintering time and hence energy can be reduced significantly using thermal plasma heating as compared to conventional heating source for sintering. It is also observed that the rate of change of density after 15 min is moderately slowed down and becomes a constant value (approximately) after certain sintering time (after 25 min not shown) for each of the plasma power. Higher plasma power brings down (reduce) sintering time for the same densification of the materials. The rate of change of physical densification is observed to be higher for higher plasma power.

Shrinkage

Figure 3a, b presents the percentage of shrinkage as a function of pellet composition in Al_x–Zr_{100-x} (x = 0, 10, 20...100) oxides sintered at different temperature with 20 h of sintering time for conventional heating and 15 min of sintering time at different power for extended arc thermal plasma heating. Identical shrinkage behaviour was observed for both type of heating. However, it is noted that high ZrO_2 content composites showed moderately larger shrinkage as compared to the Al_2O_3 rich composites. Larger shrinkage observed in Zr rich content composites within fixed interval of sintering time may be related to the faster mass flow rate in Zr rich composites under similar experimental conditions. As regard to the thermal conductivity of Zr and Al, it is noted that Zr ion has relatively higher thermal conductivity than that of Al. Hence for a particular heating temperature, heat transport capacity of Zr is larger as compared to the Al in this composite. Due to this reason, enhanced mass transport phenomena is taking place in Zr rich content composites under identical heating schedule as compared with less Al content composites. However, at the end of long range heating schedule (i.e. approx. 20 h of sintering time), the shrinkage and density behaviour remains identical.

It is important to note that higher plasma power beyond 20 kW did not enhance the physical densification significantly and percentage of shrinkage for the whole set of Al_2O_3–ZrO_2 composites for 15 min of sintering by plasma heating. Maximum density of the pellets were observed to be closed to 96% of the theoretical density. However, on further increasing sintering time upto 25–30 min, it is noted that densification achieved upto 98% (maximum). But shrinkage percentage remained almost same. Referring to this discussion of shrinkage in conventional sintering, it is noted that percentage of ZrO_2 shrinkage is always more than that of Al_2O_3. Other possible reason for this shrinkage may be due to the development of bonding characterization

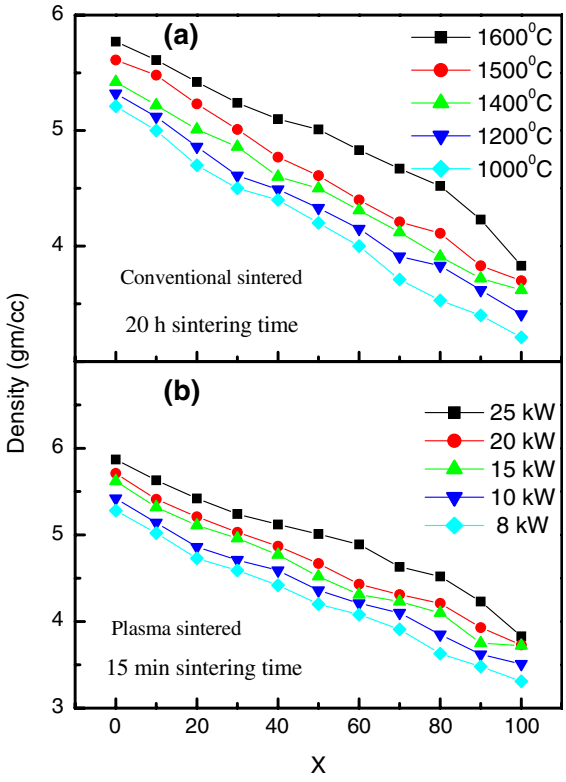

Fig. 2 Variation of sintered density with composition of Al_x–Zr_{100-x} (x = 0, 10, 20...100) oxide composites for (**a**) conventional sintered sample at different temperature at a fixed time of 20 h and (**b**) plasma sintered sample at different power at fixed sintering time of 15 min

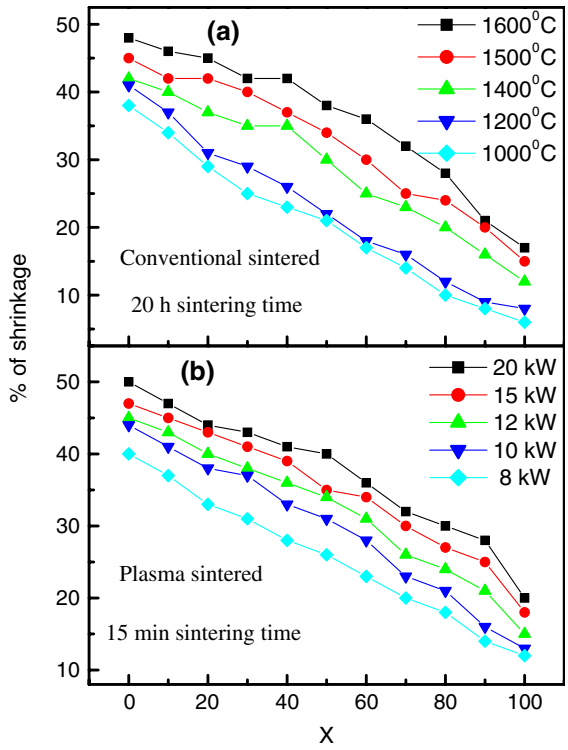

Fig. 3 Variation of percentage of shrinkage as a function of pellet composition (Al_x–Zr_{100-x} for x = 0, 10, 20...100) for (**a**) conventional sintered sample at different temperature with 20 h of sintering time and (**b**) plasma sintered sample at different plasma power with 15 min of sintering time

in ZrO_2 during solid-state reaction. Strong covalent bonding with 7 co-ordination number of ZrO_2 [28] is likely to be responsible for the maximum shrinkage during sintering as compared to the Al_2O_3.

Hardness

Variation of hardness as a function of composition in Al_x–Zr_{100-x} (x = 0, 10,20...100) oxide sintered at different temperature with 20 h of sintering time and with different plasma power with 15 min of plasma sintering time are presented in Fig. 4a, b respectively. As such pure Al_2O_3 shows higher hardness as compared to pure ZrO_2 sintered pellet. However, different composites (varying of x in Al_x–Zr_{100-x}) showed different hardness value as observed for both plasma and conventional sintered sample with varying processing conditions. Hardness of conventional sintered samples were measured for different sintering temperature and fixed time. Similarly, hardness values are also measured under identical condition with respect to conventional for plasma sintered sample with different plasma power and fixed sintering time. It is observed from the Fig. 4a, b that hardness values of plasma sintered samples are more than that of conventional sintered sample. This may be interpreted by considering the grain size of respective phases of plasma sintered sample. In fact, it is seen that average grain size of the identified phases are less than that of conventional sintered sample. Due to rapid heat and mass transfer during thermal plasma heating, grain growth is impeded and hence smaller size grain are expected to be existed in plasma sintered sample. As evident from literature, coarser grain size lead to lower hardness [29]. Smaller grain yield comparatively larger hardness value with respect to larger grain size which are possible to be grown in the conventional heating of sintered bodies for long heating schedule (20 h of sintering time).

XRD

X-ray structural analysis related to phase formation and transformation were carried out for conventional and plasma sintered Al_x–Zr_{100-x} (x = 0, 10, 20...100) oxide composites. To study the sintering behaviour of the composites, XRD pattern of pure ZrO_2 and Al_2O_3 (x = 0 and 100) were first carried out for both conventional (1600 °C for 20 h) and plasma (15 kW for 15 min) sintered sample and presented in Fig. 5. Respective phases were identified and placed in the XRD pattern, which revealed that

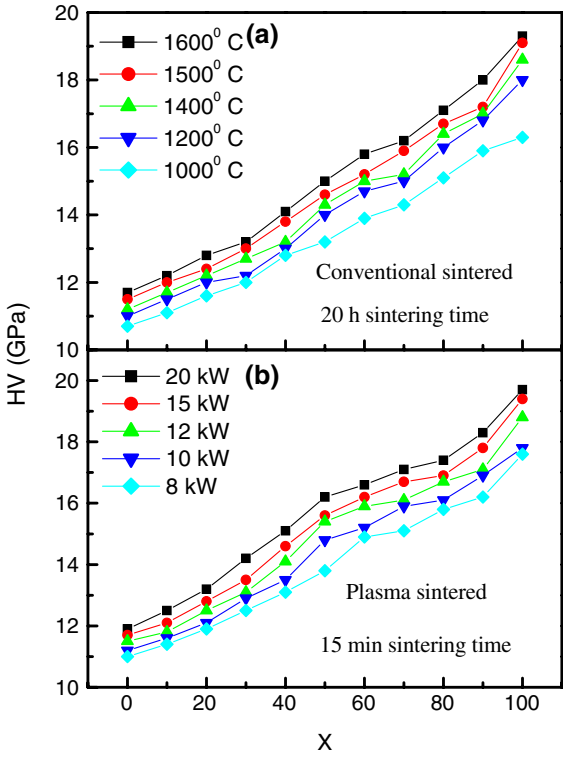

Fig. 4 Variation of hardness as a function of pellet composition (Al_x–Zr_{100-x} for x = 0, 10, 20...100) for (**a**) conventional sintered sample at different temperature with 20 h of sintering time and (**b**) plasma sintered sample at different plasma power with 15 min of sintering time

monophasic material are formed during the sintering for both pure Al_2O_3 and ZrO_2. However, plasma heated sintered sample (PHSS) always showed large I/I_0 as compared to conventional heated sintered sample for both pure Al_2O_3 (α-phase) and ZrO_2 (t-phase) materials. It is also noted that there are some extra XRD peaks exist in the pattern of PHSS. Appearance of extra peak in PHSS may be due to the sudden cooling of PHSS and high reaction rate takes place in thermal plasma heating.

XRD pattern of both conventional sintered sample (1600 °C for 20 h) and plasma sintered sample (15 kW for 15 min) were analyzed for x = 10 and 20 in Al_x–Zr_{100-x} oxides and presented in Fig. 6. It is noted that both cubic and tetragonal phases are developed for x = 10 and 20 with higher weight percent of monoclinic phase in conventional sintered sample. However, in plasma sintered sample, a few tetragonal peaks are seen to be evolved with relatively higher tetragonal intensity. This suggest that plasma heating promotes the formation of both cubic and tetragonal phase for x = 10 and 20 in Al_x–Zr_{100-x} oxide system.

From this observation, it is revealed that upto x = 20 in Al_x–Zr_{100-x} oxide system are highly preferable to form solid solution of Al–Zr oxide at high temperature and solubility is more favourable in plasma sintered sample for which we have noted the appearance of few tetragonal phase in both x = 10 & 20 composition including minor shifting (≈0.5 degree) of the selected peak position as reflected in Fig. 6. However, the solubility of this solid

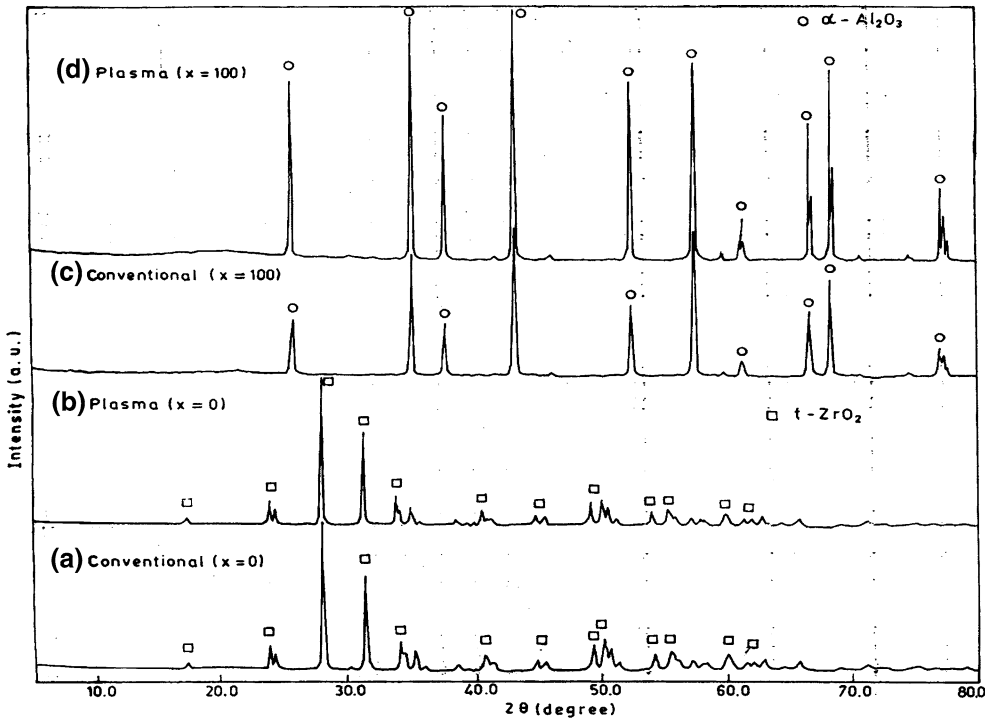

Fig. 5 XRD pattern of conventional (1600 °C for 20 h) and plasma sintered (15 kW for 15 min) sample of Al_x–Zr_{100-x} (x = 0 and 100) oxide system

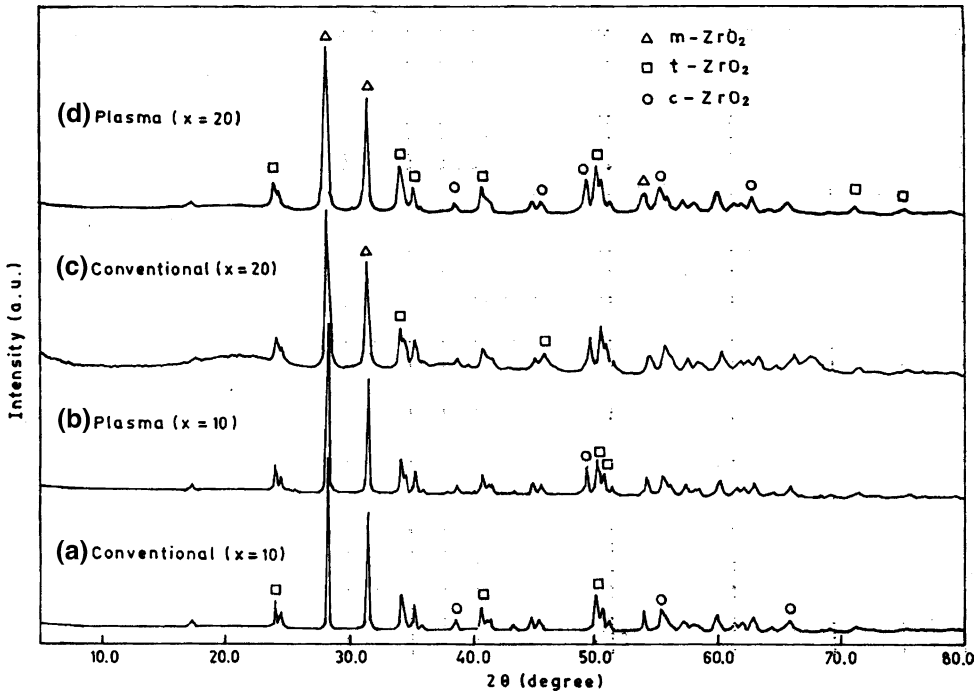

Fig. 6 XRD pattern for conventional (1600 °C for 20 h) and plasma sintered (15 kW for 15 min) sample of Al_x–Zr_{100-x} (x = 10 and 20) oxide system

solution drastically falls down in case of x = 30 composition for both conventional as well as plasma sintered sample. No solid solution of Al–Zr for x = 30 composition are formed.

It is noted from XRD intensity for x = 30 composition that sharp crystalline peaks are observed within a few minutes of sintering by plasma where as long hours (≥15 h) sintering time at 1600 °C are required to get the identical peaks. It is clearly seen from XRD that the plasma power and sintering time enhance the extent of certain phase formulation. It is also observed that two phase materials exist in conventional sintering which is basically based on monoclinic zirconia (mz) and α-Alumina (αA). However, with plasma sintering, one additional peak seems to be appear, which is tetragonal zirconia (tz). This is interesting to note that the arrest of tetragonal phase during plasma sintering is possible. The relative intensity (I/I_0) values are always larger in case of plasma sintered specimen suggesting the formation of crystalline behaviour significantly with the use of plasma process [25]. It is also observed that plasma sintered specimen formed a multi phase (mz/tz and αA) material which is of high crystalline nature within 15 min. However, the conventional sintering showed only mz and αA phases at 1600 °C sintering temperature.

In order to understand the compositional affect on phase formation and solubility of Al_2O_3–ZrO_2 composites at high temperature, XRD pattern were taken for x = 40, 50, 60 ...90 and analyzed. It is always noted that plasma sintered showed more number of X-ray reflections lines than that of the conventional one. As observed from the X-ray reflections, it is interesting to mention here that sintered products are the mixtures of both monoclinic and tetragonal phase for both plasma and conventional sintered product. However, tetragonal phase is less as compared to the monoclinic phase. Further, it is noted that in plasma sintered sample, the number of both tetragonal and monoclinic phase is more as compared to the conventional sintered sample. Both plasma as well as conventional sintered samples are similar in X-ray reflection character except the appearance of some extra peaks (X-ray reflection) at higher 2θ angle in plasma sintered sample. These extra peak reflections may be due to sample contamination caused during extended arc thermal plasma heating where graphite crucible are used to hold the sample to be sintered in presence of non reactive Ar plasmagen gas.

So from XRD analysis it is evident that major phase of monoclinic ZrO_2 always appeared in the XRD pattern for all composition (x = 30, 40 to 90) including the appearance of tetragonal phase. On the other hand α alumina phase are very much prominent as the value of x in the matrices increases.

Microstructure

A typical SEM photograph which showed an average size of 5–6 μm under sintering temperature of 1600 °C for 8 h of sintering time is shown in Fig. 7a. This fine grain size is comparable with our starting material particle size obtain from laser particle size analyzer. Hence fine grain is attributed to the increase of hardness value in the initial stage of sintering. As sintering time is increased, the grain

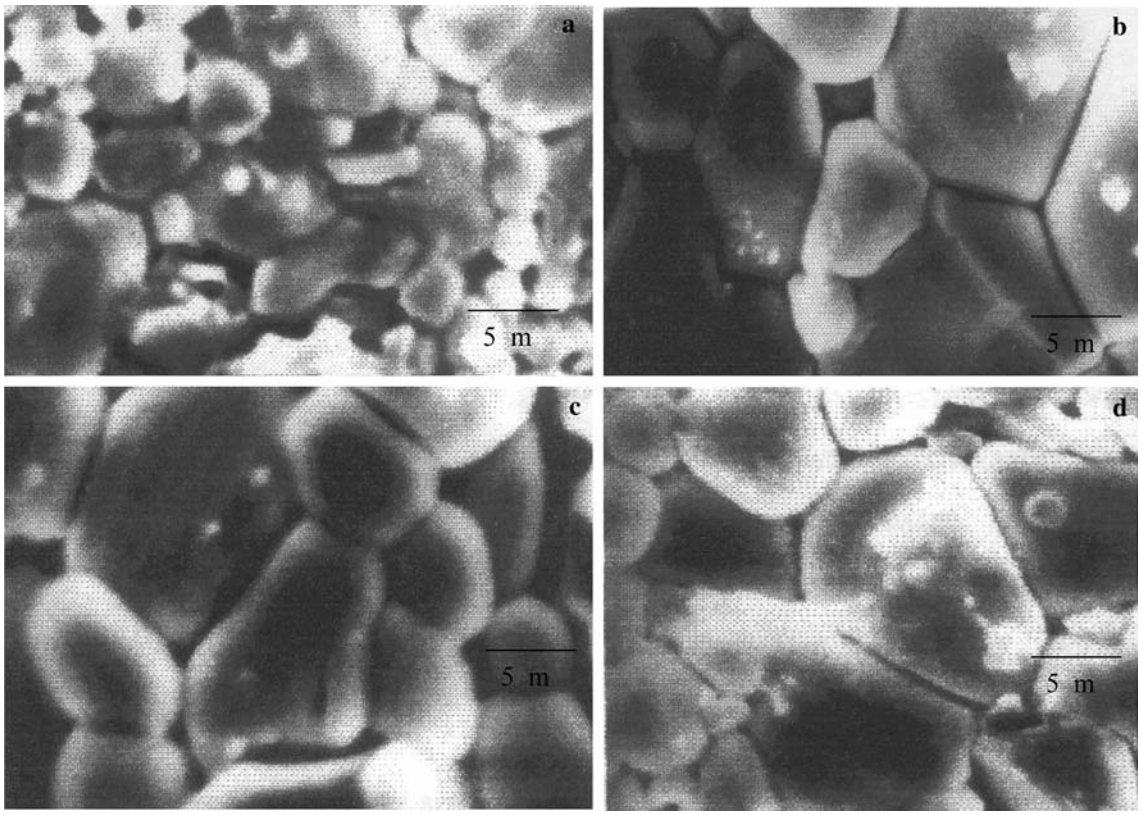

Fig. 7 SEM photograph of Al_x–Zr_{100-x} (x = 70) oxide sample conventional sintered at 1600 °C for (**a**) 8 h (**b**) 20 h and plasma sintered at 15 kW power for (**c**) 15 min (**d**) 20 min

growth started and at the same time pore formation are accelerated with the formation of triangular junction between the grains. This in turn enhances the bulk density, which is shown in Fig. 7b and yield coarser grain which reduces the HV value. Significant grain growth takes place during long range (20 h) sintering schedule carried at high temperature. In order to understand and observe the sintering process with plasma heating, SEM photograph at different plasma power and time are presented in Fig. 7c, d. As seen from Fig. 7c sintered particles are not densely populated as seen in Fig. 7d. However typical triangular hollow junctions are observed with grain boundaries. Irregular pores are also seen. As sintering time is increased, the grain structure refinement occurs and more and more clean triangular grain junctions are formed. Clear pores are noticed along the grain boundaries and in the triple junction. This may be compared to final stages of sintering of conventional sintering. The density of sintered product also increases with respect to 15 min sintering time. Dense and homogenous products are obtained for each composition within 20 min using 15 kW plasma power. It is important to observe that no significant grain growth occurred during sintering as compared with the average diameter of the green powder particle size. It is also observed from SEM picture that the average particle size varies 5–6 μm, which is identical with starting material particle size. In addition homogenous grain distribution was also observed. This observation suggest that grain growth can be controlled to a significant level during sintering by this technique within few minutes which is not possible in conventional sintering to get similar dense product after prolonged sintering (a few tens of hours). It is also observed that rapid shrinkage but no significant grain growth during sintering as compared to initial particle size. This suggest that small size particle down to nanometer scale can be sintered to achieve high density without significant grain growth.

Dielectric properties

Compositional variation of dielectric constant (K) and dielectric loss ($\tan\delta$) for both conventional sintered and plasma sintered samples are shown in Figs. 8 and 9 having experimental conditions mentioned in the respective figures. K values of pure Al_2O_3 and ZrO_2 are almost equal to their respective value in literature [30, 31] for conventional sintered sample at room temperature and at low frequency. From figure, following observations are found

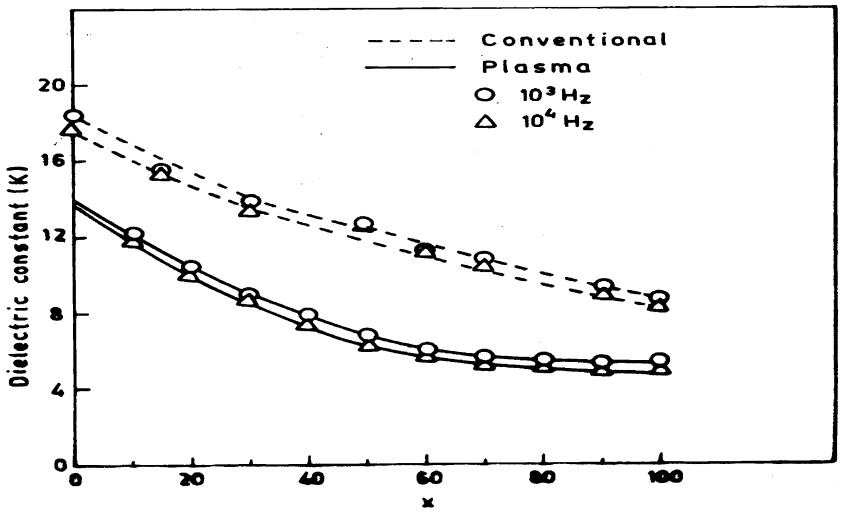

Fig. 8 Variation of dielectric constant (K) with Al_x–Zr_{100-x} (x = 0, 10, 20...100) oxide system for conventional sintered (1600 °C for 20 h) and plasma sintered (15 kW for 15 min) specimen at two different frequencies (10^3 and 10^4 Hz)

1. K & tanδ are very much frequency dependent (K & tanδ values at 10^3 and 10^4 Hz are different)
2. Plasma sintered sample always shows less K value as compared to conventional sintered sample.
3. Increasing value of x in Al_x–Zr_{100-x} oxide composites always decreased the value of K even if sintered by plasma heating or conventional heating.

The dielectric constant (K) at low frequencies depends on the excitation of bound electrons, lattice vibrations, dipole orientation, and space-charge polarization (atomic or electronic). At very low frequencies, all four contributions may be active. The manner of variation of dielectric constant with frequency indicates which contributions are present. All four types of polarization can be correlated to ''oscillators'' with specific eigenfrequencies and damping. The ''eigenfrequencies of oscillators'' play [32] the essential role.

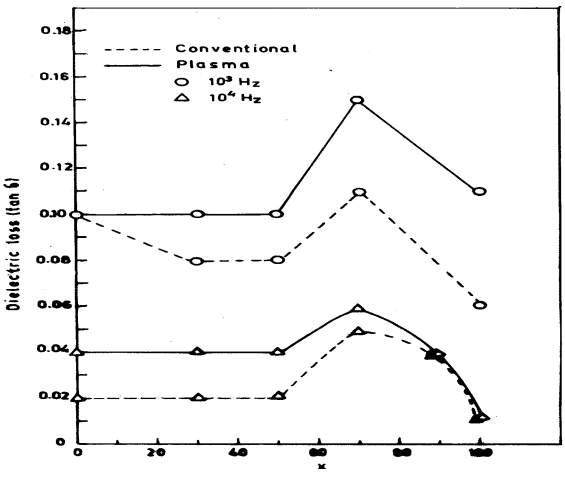

Fig. 9 Variation of dielectric loss (tanδ) with Al_x–Zr_{100-x} (x = 0, 10, 20...100) oxide system for conventional sintered (1600 °C for 20 h) and plasma sintered (15 kW for 15 min) specimen at two different frequencies (10^3 and 10^4 Hz)

In nonhomogeneous materials and mixtures, the interfacial polarization (also known as Maxwell–Wagner–Sillars polarization) is present [33–35] due to the differences between the electrical properties of the constituents. This polarization can also be assumed to be a molecular polarization proposed by Onsagar [36].

The simplest correlation between dielectric constant and frequency is given by the Debye equation [37]

$$K(\omega) = K_\infty + (K_s - K_\infty)/[1 + (\omega\tau)^2]$$

where K_∞ = dielectric constant far above the frequency ω, K_s = static dielectric constant, $\omega = 2\pi v$, and τ is the relaxation time of strongly damped oscillators. In this equation the frequency appears explicit, while the temperature is implicit in K_s, K_∞, and τ. Since our dielectric measurements are in low frequency region from 10^2 to 10^5 Hz, the contribution of bound electrons and atoms results mainly in the high frequency part which can be expressed $K_{\infty =} K_e + K_a$. However, according to Szigeti [38] the electronic and atomic polarizations are not independent. The influence of electronic polarization on atomic polarization is twofold: long-range and short range interaction. Both parts increase with K_∞. Numerical evaluation is not possible because the values of the involved parameters and their interrelation are not well known.

The vibrational contribution can be less or more than the electronic contribution, depending on the spectral position of the eigenfrequency of electronic and atomic oscillators. The contribution of space charge will depend on the purity and perfection of materials. Its influence will be noticeable mainly in the low-frequency region.

From the analysis of the dielectric spectrum, this increase of K value at low frequency (10^2 Hz) can be

explained by space charge polarization caused by impurities or material defects [32] in form of voids or pores present at microscopic level. Of the several possible polarization mechanism to explore the observed dielectric spectrum, induced atomic or electronic, and also ionic lattice polarization respond so rapidly that they are effectively instantaneous below certain high frequencies, contributing a purely real value of K_∞, to the permittivity. Permanent molecular dipoles, ionic defects of dipolar type (vacancy—interstitial pairs) and also slowly mobile hopping charge carriers of electronic, polaronic or ionic nature may produce much slower responses to this system of composition where both ZrO_2 and Al_2O_3, phases having their own internal phase transformation.

In order to understood further for the contributions of polarization mechanism, both Dielectric constant (K) and loss ($\tan\delta$) as a function of frequency for both plasma and conventional sintered sample of Al_x–Zr_{100-x} oxide system are studied. It is observed that the variation behaviour of both K and $\tan\delta$ are identical with respect to frequency variation. The value of K is reduced at low frequencies down to 40–45% of its conventional sintered sample and bearing a semi straight line character. The flatness behaviour of dielectric response in plasma sintered sample strongly suggest that there is no space charge polarization mechanism involved [24] in plasma sintered sample. This simple dielectric spectra observed for plasma sintered sample with no space charge polarization [24, 32] may be the primary reason for the reduction of K values significantly as compare to conventional sintered sample. Hence it is concluded that space charge polarization is prominent in conventional sintered sample but not in plasma sintered sample for which there is a reduction of K values in different x value of the composition in Al_x–Zr_{100-x} ceramic oxides. Reduction of K value are also reported by many author in thin film form of Al_2O_3 [39]. Decrease in K is believed to be arising from the increase of void density. Several authors [40, 41] have reported that due to the effective thickness of insulators, the value of K decreases with increasing void density. However, in plasma sintered sample, this densification rate has been approached ≥98% and the presence of void and its role may be insignificant. Hence, contribution of void at microscopic level for the reduction of K value by plasma is ruled out. In this situation, it may be appropriate to consider the voids/porosity or inclusion at the nanoscopic range. Due to sudden rise of high temperature in thermal plasma heating reactor, above proposed entity may be generated at angstrom or nanometer range. Inclusion may also plays important role in reducing the value of K for plasma sintered sample. It is also anticipated that inclusions are incorporated with enhanced density into the matrix by thermal plasma heating as compared to conventional heating. The exact cause for the reduction of K at this stage is not known. No other research reports appears to have been reported by any other researcher along this line and hence more experimental evidence and observation are required to understand this reduction mechanism of K.

Low temperature measurements of both K and $\tan\delta$ were also taken at 77 K using liquid nitrogen cryostat for both conventional and plasma sintered pellets of different Al_x–Zr_{100-x} (x = 0, 10, 20...100) composites. It is noted that value of the K and $\tan\delta$ are changed with marginal decrease with respect to the room temperature value of the same composition. However, the nature and trend of K and $\tan\delta$ remain the same at per with room temperature data. This marginal decrease of both K and $\tan\delta$ values may be due to the rigidity of dipole orientation under the influence of electric field at low temperature. Similar results are also obtained for conventional sintered Al_x–Zr_{100-x} sample for K and $\tan\delta$ measurements at 77 K. It is interesting to note that the values of K are reduced marginally as compared to plasma sintered sample at room temperature. This reduction may similarly be interpreted as above. Further details dielectric and its related structural and microstructural studies are very much essential to understand the real mechanism in this high temperature plasma sintered oxide composites.

Conclusion

Highly dense (close to theoretical value) sintered materials of Al_2O_3–ZrO_2 oxides with greater hardness including homogenous phase distribution are prepared using EATPH technique. Grain growth rates for all composites are highly restraint by EATPH and the sintered product culminates with much finer microstructure due to high heat and mass transfer kinetics in thermal plasma heating. So this thermal plasma heating technique may be extended to process nanostructure where grain growth is practically not recommended. Dielectric constant can be reduced significantly using this plasma heating technique, which may be used to tailor ultra low K dielectric material.

Acknowledgement Author D. R. Sahu is thankful to Director Institute of Materials Science, Bhubaneswar for giving permission to visit National Cheng Kung University, Tainan, Taiwan for a research assignment.

References

1. Bykov YV, Rybakov KI, Semenov VE (2001) J Phys D: Appl Phys 34:R55
2. Jones RH (1993) JOM December 14
3. Willert-Porada MA et al (1997) In: Shiota I et al (eds) Functionally graded materials 1996. Elsevier, Amsterdam p 349

4. Horano H, Inada H (1992) J Mat Sci 27:3511
5. Saha A, Agarwal DC (1998) J Mat Sci 77:1333
6. Bykov YV, Rybakov KJ, Semenov VE (2001) J Phys D: Appl Phys 3:255
7. Kim JS, Jhonson DL (1983) Ceramic Int 82(5):620
8. Bensisu K, Inal OT (1994) J Mat Sci 29:5175
9. Kakegawa K, Uekawa N, Wu YJ, Sasaki Y (2003) Mat Sci Eng B 99:11
10. Nicolas G, Austric M, Marine W, Hefev GA (1997) App Sur Sci 109/110:289
11. Zhang YL, Jin XJ, Hsu TY, Zhang YF, Sli JL (2001) Scripta Materilia 45:621
12. Reyes Morel PE, Chen IW (1988) J Am Ceram Soc 71:648
13. Von Recum AF (1998) Handbook of biomaterials evaluation, 2nd edn. CRC publication, p 143
14. De Aza AH, Chevalier J, Fantozzi G, Schedi M, Torrecillas R (2002) Biomaterials 23:937
15. Willmann G (2000) Adv Eng Mater 2:114
16. Cutler RA, Reynolds JR, Jones A (1992) J Am Ceram Soc 75(8):2175
17. Lee JK, Hang HH (2001) Mat Lett 42:215
18. Oh HS, Tomadel G, Le WH, Choi SC (1996) J Mat Sci 31:5321
19. Johnson DL (1969) J Appl Phys 40(1):192
20. Johnson DL, Cutler JB (1963) J Am Ceram Soc 46:541
21. Johnson DL, Rizzo A (1980) J Am Ceram Soc 55(4):380
22. Johnson DL (1983) Proceedings of the international symposium on ceramic composites for engine. Hakone, Japan
23. Roul BK, Singh SK, Mohanty BC (1998) J Mat Synt Proc 6:9
24. Sahu DR, Roul BK, Singh SK, Choudhury RNP (2002) J Mat Design Appl L2 216:127
25. Roul BK, Sahu DR, Mohanty S, Mohanty BC, Singh SK (2001) Mat Chem Phys 67(1/3):151
26. Sahu DR, Singh SK, Choudhury RNP, Roul BK (2004) Mat Sci Engg B 106:141
27. Sahu DR, Roul BK, Singh SK, Choudhury RNP (2002) Mat Lett 56:817
28. Shim Ming Ho (1982) Mat Sci Eng 54:23
29. Hong J, Gao L, Torre SDDL, Miyamoto H, Miyamoto K (2000) Mat Lett 43:27
30. Thompson DP, Dickins AM, Thorp JS (1992) J Mat Sci 27:2267
31. Molla J, Hridinger R, Ibarra A, Link G (1993) J Appl Phys 73(11):7667
32. Rao KV, Smakula A (1965) J Appl Phys 16(6):2031
33. Sillars R (1937) J Inst Elec Eng 80:378
34. Maxwell JC (1891) A treatise on electricity and magnetism, 3rd edn, vol. 1. Clarendon, Oxford (reprint by Dover)
35. Wagner KW (1914) Arch Elektrotech (Berlin) II 371
36. Onsager L (1936) J Am Chem Soc 58:1486
37. Debye P (1929) Polar molecules. Chemical Catalog Company, New York
38. Szigeti B (1949) Trans Faraday Soc 45:155; (1950) Proc Roy Soc London, A 204:51; (1959) A252:217; (1960) A258:377
39. Chopra KL (1969) Thin film phenomena. McGraw-Hill, New York
40. Sexena U, Srivastava UN (1976) Thin Solid Films 33:185
41. Weaver C (1965) Vacuum 15:171